Boundary-Layer Meteorology

A mesoscale model-based climatography of nocturnal boundary-layer processes over the complex terrain of northwestern Utah

--Manuscript Draft--

Manuscript Number:	
Full Title:	A mesoscale model-based climatography of nocturnal boundary-layer processes over the complex terrain of northwestern Utah
Article Type:	Research Article
Keywords:	Stable boundary layers; Mountain meteorology; Boundary layer separation; MATERHORN Project
Corresponding Author:	Stefano Serafin AUSTRIA
Corresponding Author Secondary Information:	
Corresponding Author's Institution:	
Corresponding Author's Secondary Institution:	
First Author:	Stefano Serafin
First Author Secondary Information:	
Order of Authors:	Stefano Serafin
	Stephan F.J. De Wekker
	Jason C. Knievel
Order of Authors Secondary Information:	
Abstract:	Nocturnal boundary-layer phenomena in regions of complex topography are extremely diverse and respond to a multiplicity of forcing factors, acting primarily on the meso- and micro-scale. The interaction between different physical processes, e.g., drainage promoted by near-surface cooling and ambient flow over topography in a statically stable environment, may give rise to special flow patterns, uncommon over flat terrain. This study presents a climatography of boundary-layer flows, based on a two-year archive of simulations from a high-resolution operational mesoscale weather model, 4DWX. The geographical context is Dugway Proving Ground, in northwestern Utah (USA), target area of the field campaigns of the MATERHORN project. The comparison between model output and available observations in the 2012--2014 period shows that 4DWX provides a realistic representation of wind speed and direction in the area, at least in an average sense. Regions displaying strong spatial gradients in the field variables, thought to be responsible for enhanced nocturnal mixing, are sought and found to be typically located in transition areas from mountain sidewalls to adjacent plains. A key dynamical process in this respect is the separation of dynamically accelerated downslope flows from the surface.
Suggested Reviewers:	Dragan Zajic dragan.zajic.civ@MAIL.MIL Meteorologist at DPG (field site of MATERHORN-X)
	Branko Grisogono bgrisog@gfz.hr Expert on stable boundary layers
	Qingfang Jiang qingfang.jiang@nrlmry.navy.mil Extensive previous work on boundary layer separation
	Simon Vosper

	simon.vosper@metoffice.gov.uk Mountain meteorology expert
	John Horel john.horel@utah.edu Mountain meteorology expert, based in Utah

Noname manuscript No.
(will be inserted by the editor)

A mesoscale model-based climatography of nocturnal boundary-layer processes over the complex terrain of northwestern Utah

Stefano Serafin · Stephan F.J. De Wekker · Jason C. Knievel

Received: date / Accepted: date

Abstract Nocturnal boundary-layer phenomena in regions of complex topography are extremely diverse and respond to a multiplicity of forcing factors, acting primarily on the meso- and micro-scale. The interaction between different physical processes, e.g., drainage promoted by near-surface cooling and ambient flow over topography in a statically stable environment, may give rise to special flow patterns, uncommon over flat terrain. This study presents a

S. Serafin
Department of Meteorology and Geophysics, University of Vienna, Vienna, Austria
Tel.: +43-1-4277-53711
Fax: +43-1-4277-8-53711
E-mail: stefano.serafin@univie.ac.at

S.F.J. De Wekker
Department of Environmental Sciences, University of Virginia, Charlottesville, Virginia

J. Knievel
National Center for Atmospheric Research, Boulder, Colorado

climatography of boundary-layer flows, based on a two-year archive of simulations from a high-resolution operational mesoscale weather model, 4DWX. The geographical context is Dugway Proving Ground, in northwestern Utah (USA), target area of the field campaigns of the MATERHORN project. The comparison between model output and available observations in the 2012–2014 period shows that 4DWX provides a realistic representation of wind speed and direction in the area, at least in an average sense. Regions displaying strong spatial gradients in the field variables, thought to be responsible for enhanced nocturnal mixing, are sought and found to be typically located in transition areas from mountain sidewalls to adjacent plains. A key dynamical process in this respect is the separation of dynamically accelerated downslope flows from the surface.

Keywords Stable boundary layers · Mountain meteorology · Boundary layer separation · MATERHORN Project

1 Introduction

Granite Peak, located in the Dugway Proving Ground (DPG) in northwestern Utah, is an isolated mountain rising ∼800 m above the surrounding terrain (Fig. 1). It has an approximately ellipsoidal shape oriented NNW-SSE, and its main axes are respectively ∼10- and ∼6-km long. A flat salt plain (*playa*) lies west and northwest of the peak. To the east lies a broad valley gently sloping towards the northwest, covered by herbaceous vegetation. This arid grassland is surrounded almost completely by other prominent peaks—the

Cedar Mountains to the northeast, Indian Peaks to the southeast, and the Dugway Range to the southwest.

{Figure 1 here}

On nights with weak synoptic flow, these topographic features are favourable for the onset of diverse local wind systems in the atmospheric boundary layer (BL). In particular, the cooling phase of the diurnal cycle generates drainage flows. Furthermore, stable stratification down to the ground promotes a variety of dynamically forced phenomena. When the upstream flow conditions support the onset of propagating mountain waves, the related local pressure minima on the leeside slopes of mountains contribute to the downslope acceleration of ambient winds (Nappo 2013). Dynamically accelerated downslope winds are not necessarily intense and damaging, but they originate from essentially the same type of forcing that causes downslope windstorms at many locations around the world, e.g., the northeastern Adriatic Sea (Bora winds, Grisogono and Belušić 2009), the foot of Colorado's Front Range (Lilly 1978), or Owens Valley in California, east of Sierra Nevada (Grubišić et al 2015a).

Pressure perturbations embedded in mountain waves can be strong enough to force the atmospheric BL to separate from the ground near the foot of mountain slopes (French et al 2015; Grubišić et al 2015b) and, in extreme cases, develop highly turbulent rotors (Grubišić et al 2008). The formation of atmospheric wakes (Epifanio 2003) and gap flows (Mayr et al 2007), especially at the rather narrow constriction separating Granite Peak from the northwestern tip of the Dugway Range, are among the other phenomena expected to occur in this area under statically stable conditions.

The interaction between (dynamically forced) downslope winds and (thermally forced) drainage flows in the vicinity of Granite Peak and elsewhere in DPG is far from obvious, and may frequently lead to convergence lines or collisions between airmasses with markedly different properties (Dimitrova et al 2015). These type of events are expected to generate vigorous mixing even during the night, in contrast to the typical behaviour of stable BLs over flat terrain.

Beyond topography, also landuse variability at DPG plays a role in generating thermally driven flows. The most prominent is diurnal flow from the playa to the sagebrush plain, induced by differences in sensible heat flux between the two environments. In analogy to sea- and lake breezes, circulations arising from differential heating in such conditions have occasionally been referred to as “salt breezes” (Physick and Tapper 1990; Rife et al 2002).

The possible occurrence of such a wide range of weather phenomena, as well as the nontrivial interaction between them, make this area an ideal location to make progress in understanding the properties of multiscale mountain flows. Two field campaigns related to the MATERHORN project took place in DPG in fall 2012 and in spring 2013 (Fernando et al 2014). Special instrumentation deployed during the project complemented an existing permanent mesoscale network of surface measurement stations (SAMS), with an average density of approximately 1 station every 100 km^2, extending over the whole of DPG and the immediate surroundings. A second network with considerably higher density (Mini-SAMS, 1 station every 2 km^2) covers a limited area in the valley east of Granite Peak. Operational high-resolution numerical weather prediction products are also continuously available at DPG from the 4DWX forecast system developed by the NCAR Research Applications Laboratory (Davis et al 1999; Liu et al 2008), which provides eight daily runs with hourly model output.

In this study, simulations from the 4DWX system in the DPG domain are used to build a short-term climatographical characterization (2012–2014) of nocturnal BL phenomena in the area. The purposes of the study are manifold. First, it is expected that insights resulting from the analysis can, if necessary, be exploited in designing and implementing field studies at DPG. Second, quantitative knowledge of the typical flow phenomena in a given area and of their modulation by topography and land-use features is advantageous in the correct interpretation of measurements and in the generalization of results from case studies. Third, information about the average wind climate of a given area provides a context for the formulation of scenarios for idealized simulations (e.g., aimed at understanding specific processes), or for applied studies (e.g., to model pollutant or tracer dispersion).

The paper is organized as follows. Sections 2 and 3 introduce and compare measurements from the SAMS network and 4DWX simulations. The prevailing wind regimes at DPG and the diurnal variability of wind direction at a few selected sites are discussed therein. Section 4 focuses on seeking preferential areas for flow convergence or boundary layer separation (BLS). Discussions and conclusions are included in Section 5.

2 Data and methods

2.1 Observational data

Near-ground observations are from the SAMS (Surface Atmospheric Measurement Systems) stations operated by DPG. A SAMS station typically comprises probes that measure temperature and relative humidity at 2 m AGL and vane anemometers that measure wind speed and direction at 2 and 10 m AGL. SAMS data used in the present study are from the two-year period between 1 July 2012 and 30 June 2014. Data are available as 5-minute averages and data availability exceeds 90% at most of the 31 stations, except for two that were installed only recently. Vane anemometer measurements from Mini-SAMS stations from 15 September to 29 October 2012 (during the Materhorn fall 2012 field campaign), with 1-minute resolution, were also considered.

2.2 4DWX

Since the 1990s, DPG has used a continuously operating meso-gamma-scale analysis and forecast system (4DWX) developed by the NCAR Research Applications Laboratory (Davis et al 1999; Liu et al 2008). Largely sponsored by the U.S. Army Test and Evaluation Command, 4DWX is in use at eight different test ranges in the United States. While the primary use of the modelling system is weather forecasting, coupled applications for pollutant dispersion modelling and noise assessment (Sharman et al 2008) are also operated. The DPG implementation of the system is currently based on version 3 of the Advanced Research core of the WRF model (Skamarock and Klemp 2008), runs with a grid spacing of 1.1 km in the innermost of 4 domains, and provides weather analyses and forecasts at hourly intervals. Eight forecast cycles are run every day. Simulations starting at hour t (real time) are initialized at time $t-3$ and are nudged toward observations during the first three hours of the run, from $t-3$ to t. The initial hours of all runs, taken consecutively, form a continuous final analysis (Liu et al 2008) whose output is considered in the present study. The 4DWX data used here are from 1 July 2012 to 30 June 2014. Model output at hourly resolution is available for almost all days during the two years (16588 out of potentially 17520 outputs, i.e., $\sim$94.6%), the few gaps being due to maintenance or unexpected downtime of the computing infrastructure.

The physics parameterizations for the WRF model in 4DWX include the Yonsei University (YSU) boundary-layer scheme (Hong et al 2006), the Noah land-surface model (Chen and Dudhia 2001), the Monin-Obhukov surface-layer scheme (Janjič 2002), the Dudhia scheme (Dudhia 1989) for short-wave radiation, the Rapid Radiative Transfer Model (Mlawer et al 1997) for long-wave radiation, the updated Kain-Fritsch cumulus scheme (Kain 2004), and the Thompson microphysics scheme (Thompson et al 2004). Explicit sixthorder diffusion is applied to suppress noise in kinematical fields, especially in near-neutral boundary layers under weak winds (Knievel et al 2007).

The 4DWX simulation domains are displayed in Fig. 1. The 1.1-km domain is centered on the sagebrush plain east of Granite Peak and its horizontal mesh consists of 60×60 grid points. Flow relaxation is imposed within five grid points from all lateral boundaries in order to enforce boundary conditions by means of Newtonian nudging. Because of this, the wind field is not in exact balance with the pressure field and the other source terms in the area outside the core region. This outer "halo region" is therefore discarded in all the analyses presented in this paper.

3 Observed and modelled wind climate

3.1 Comparison between observations and simulations

An exhaustive verification study of 4DWX simulations is beyond the scope of the present study. Rather, what is of interest to us is the model's ability to reproduce, in a climatological sense, the observed wind variability in the area. Therefore, rather than concentrate on individual days or case studies, we try to determine the level of confidence by which 4DWX can reproduce the general character of the near-surface atmospheric circulation, e.g., variability in wind speed and direction. Hourly measurements from a few selected stations in the SAMS network are used as the observational counterpart.

Figure 2 presents joint frequency distributions (i.e., two-dimensional histograms) of the west-east and south-north wind components at three SAMS stations and at their respective nearest-neighbor grid points in the 4DWX domain. These diagrams provide essentially the same information as wind roses, but allow a better appreciation of flow regimes that are only poorly represented in the sample. The three selected measurement stations are numbers 2, 12, and 23, lying respectively in the wide gap separating Granite Peak and the Dugway Range, in the sagebrush plain east of Granite Peak, and at the foot of the southwestern slope of the Cedar Mountains. These three locations are prototypical of the different flow patterns expected at DPG: gap flow at station 2, nocturnal drainage at station 12, and dynamically accelerated downslope winds at station 23. Although not shown here, statistics from other stations were also examined, to ensure that the three selected ones are adequately representative. For instance, the nearby Stations 4 and 12 have very similar wind direction and speed statistics, although nocturnal drainage at the valley bottom appears to be more persistent at the former. Similarly, stations 23 and 13 both show signatures of downslope flows (more frequent at the latter), although the local orientation of the slope is different.

{Figure 2 here}

The most frequent wind direction at station 2 is WSW (positive u and v components, direction approximately 240°). Wind speeds in this directional range, which corresponds to gap flow into the Dugway Plain, are typically below 5 m s^{-1}. Flows with an easterly component, i.e., into the salt plain, are also observed, but generally have a lower wind speed and a somewhat larger directional variability. Strong wind events, with wind speed up to and beyond 15 m s^{-1}, are much less frequent and related to completely different prevailing wind directions: southerly ($\sim$200°) and northerly (340° to 20°). These directions do not correspond to the main axis of the gap, but are approximately parallel to the sidewalls of nearby orography features, probably evidence of stable air masses frequently flowing around obstacles.

At station 12, the main lobes of the frequency distribution of wind components are elongated from NW to SE, along the direction of the gentle valley slope. The most frequent directions are between 90° and 180° (negative u, positive v), with wind speed mostly below 5 m s^{-1}, likely related to nocturnal drainage or to synoptic-scale southerlies dominant in the area (see below). Relatively stronger winds also seem to be preferentially southeasterly (150°), although they can occur from almost all sectors.

Station 23, located at the foot of the Cedar Mountains, displays a larger wind-direction variability than the other two stations. Even in this case, the most frequent wind direction (E) seems to be related to local modification of the prevailing southerly large-scale winds. Strong winds may blow equally frequently from almost all directions, but with a distinct preference for the northeasterly (30°), a possible hint at windstorms down the SW slope of the Cedar Mountains.

Visual comparison between measurements and 4DWX simulations indicate good agreement in the representation of both the most frequent wind directions and the typical wind speeds. The overall impression is that the set of simulations from 4DWX is a reliable representation of the observed wind climate. Similar considerations apply to almost all other SAMS stations in the area, with a few expected exceptions (like, for instance, station 16 atop Cedar Mountains).

Histograms in Fig. 2 do not discriminate between diurnal and nocturnal flow patterns. The diurnal cycle of wind directions at stations 2, 12, and 23, and at the respective closest model grid points, is therefore depicted in Fig. 3. (Only wind speeds greater than 1 m s^{-1} are considered.) Apart from the clockwise bias in simulations at station 23, the diurnal cycle of wind direction in output from 4DWX is quite realistic.

{Figure 3 here}

Taking seasonal variability into account, nighttime at DPG corresponds approximately to the period between 3 and 15 UTC. Sunrise and sunset times range respectively from 1259 to 1449 and from 0005 to 0303 UTC (from 0559 to 0749 and from 1705 to 2003 LST). At all three stations, the distribution of wind directions in nocturnal hours shows a well defined primary direction (240° at station 2, 140° at station 12, 90° at station 23) and a few equally well defined secondary directions (e.g., 0°, 120° and 190° at station 2, 330° at station 12, 30° at station 23). The primary direction corresponds to the main axis of the gap between Granite Peak and the Dugway Range at station 2, to drainage along the NW-oriented Dugway Plain at station 12, and to eastward deflection of nocturnal southerlies at station 23. Secondary directions at station 2 likely correspond to blocked flow running parallel to either Granite Peak or the Dugway Range and ultimately flowing into the gap, while the secondary direction at station 23 is related to downslope flow from the Cedar Mountains (see Fig. 1).

Due to the predictable behaviour of cool and stable air, the prevalent nocturnal wind directions are sharply defined and seemingly easy to relate to topography features. In contrast, larger variability in wind direction can be found during the daytime: wind can blow with almost uniform probability from any direction at station 2, or from anywhere between 140° and 330° at station 23. Bimodal distributions of wind directions in the afternoon hours are to a certain degree visible at all stations. At station 12, in particular, the two main branches clearly correspond to the NNW and S directions, typical of synoptic weather systems in the area. Flow from the NNW sector during daytime might be explained at least partially by upvalley flow, but NNW winds occur even at night and are somewhat frequent even at station 23, making attribution to local thermal forcing rather doubtful. A gradual clockwise rotation of the wind direction in early morning hours is apparent at station 23, consistent with a morning transition regime and the local onset of upslope flow towards the Cedar Mountains.

Diurnal cycle statistics computed from 4DWX simulations generally agree well with obervations despite some minor discrepancies, e.g., the SE rather than E direction of nocturnal flows at station 23, or the more frequent occurrence of southerly flows in the night at station 2. The encouraging results of pointwise comparisons between simulations and observations justify looking with confidence at statistics calculated over the whole core area of 4DWX domain 4.

3.2 4DWX wind climate

The relative frequency with which 4DWX simulates wind from eight directional sectors is represented in Figure 4. Sectors are 45° wide and centered on the 0°, 45°, 90°, etc., directions. Only wind speeds greater than 1 m s^{-1} are considered and no distinction between nighttime and daytime is made. It is apparent that S or SE and N or NW winds dominate the wind climate in the region. However, topography influences the local variability.

{Figure 4 here}

While N and S flows are more frequent over the playa, the dominant wind directions in the wide valley between Granite Peak and the Cedar Mountains are NW and SE, possibly as a consequence of flow channelling and/or thermal forcing. The most frequent wind direction in the gap between Granite Peak and Dugway Range is southwesterly, i.e., aligned with the main axis of the gap and into the Dugway Plain. Gap flow along the opposite direction is also found, but much less frequently.

Southerly winds are very frequent on the northern slope of the Dugway Range, but relatively uncommon immediately north of it. This suggests that downslope flows often tend to detach from the surface at the foot of the mountain without extending over the plain. Local forecasters often observe a pulse of southerly flow that crosses the plain just after sunset, after which the wind becomes very light or calm and so remains throughout the night (Matt Jeglum, personal communication). Similar considerations are valid for the northern slope of Granite Peak. Frequent flow separation and related convergence lines are expected at these locations.

Winds from the E and NE are generally rare, but comparatively more frequent on the southwestern slope of the Cedar Mountains. Locally, a spur detaching from the main ridge of the Cedar Mountains steers the predominant SE flows to E. Similarly, the frequent southwesterly flows in the gap between Granite Peak and the Dugway Range might be caused by the eastward deflection of locally dominant southerlies.

Flow around Granite Peak is common, as clearly evident in a number of diagrams. For instance, NW and SE flows are more frequent along the NE and SW sidewalls of the mountain than along the NW and SE ones. Similarly, S and N flows are more common on the E and W sides of the obstacle than on the S and N ones.

Like wind direction, extreme wind speed appears to be tightly connected to topography, as apparent in Fig. 5. The two panels display the spatial distribution of wind speeds respectively greater than the 99th and smaller than the first percentile in the whole DPG area. High wind speeds are much more frequent at mountain tops than above plains, as could be easily expected. However, they are also frequent on mountain slopes (e.g., on the SW flank of the Cedar Mountains or NW of Camelback Mountain, i.e., of the low hill at approximately $x = 38$ km and $y = 14$ km), suggesting dynamically induced downslope acceleration. Extreme wind speeds tend to develop more frequently on the slopes of the Cedar Mountains than of Granite Peak. This is presumably related to the different vertical aspect ratio of the two ridges. Stable airflow over Granite Peak, which is narrow and steep, falls more easily in the potential flow regime, in which maximum wind speeds occur right at the mountain top (Lin 2007). Instead, airflow over the Cedar Mountains, which are considerably broader and slightly lower, apparently favors vertically propagating waves and concomitant downslope acceleration.

{Figure 5 here}

Low wind speeds (Fig. 5b) are infrequent at mountain tops, while they occur most commonly over the plains closest to mountain slopes, in particular north of the Dugway Range. Flow stagnation or convergence at these locations is likely related to downslope flow separation, as explained extensively in Section 4 below.

To gain insight on the typical features of the vertical atmospheric profile in the area, histograms representing the variability of stratification (in terms of the Brunt-Väisälä frequency) and of wind direction with height, at the centre of 4DWX domain 4, are shown in Figure 6. Figures 6a and 6b show that stable stratification ($N^2 \approx 10^{-4}$ s^{-1}) and persistent W or SW winds occur in the mid-troposhere, above 4000 m MSL, as typical in midlatitudes. A larger variability both in stratification and in wind direction is found at lower altitudes, in particular between 2000 and 4000 m MSL, presumably related to synoptic weather systems. Two distinct branches of S and NW winds are in fact apparent, characterized respectively by veering (warm advection) and backing (cold advection) with height. At low altitudes (below 2000 m MSL, within a few hundred meters above ground), both southerlies and northwesterlies have a tendency to veer with height. Since this range of altitudes often corresponds to a well-mixed layer, this latter feature is likely due to the balance established between frictional and rotational effects (Ekman spiral).

{Figure 6 here}

Part of the variability in N below 4000 m is related to the occasional development of a deep convective bounday layer (CBL) during daytime. Fig. 6c and 6e provide evidence that mixed layers ($N^2 \sim 0$ s^{-2}) might grow up to an altitude of ∼4500 m (i.e., to a thickness of ∼3000 m). A detailed analysis of the spatial and temporal variability of the depth of the convective boundary layer in the DPG area is provided in De Wekker et al (2015). At night, especially within 300 m from the ground, very stable layers with N^2 up to $\sim 8 \times 10^{-4}$ s^{-2} might form.

The variability of the wind direction profiles is less obvious. Winds from the southerly sector tend to have a consistent direction below 3000 m during daytime hours (Fig. 6d) and to be subject to stronger frictional veering at night (Fig. 6f), possibly as a consequence of the diurnal variability of stratification. The more frequent occurrence of NNW winds during daytime is apparent, but attribution of this feature to the occurrence of a playa breeze or to upvalley flow remains uncertain. Rare and almost exclusively nocturnal easterlies are also apparent in Fig. 6b-d-f, most likely connected to drainage or dynamically forced flow from the Cedar Mountains' western slope, which might occasionally extend as far as the middle of the sagebrush plain.

To summarize, the 4DWX simulations suggests that some of the BL structure at DPG is largely determined by predictable mesoscale circulations generated by the topography or by land-surface inhomogeneities. However, especially during the nighttime, interaction with the dominant synoptic flow regimes (e.g., southerly or north-westerly winds) appears to be responsible for additional phenomena, like flow diversion around topography and dynamically accelerated downslope flow, mostly confined to the northern or northeastern flanks of mountains.

Results presented in this Section provide a compact summary of the prevalent wind regimes in the DPG area, but cannot elucidate the respective forcing factors thoroughly. Conclusive evidence on what are the driving mechanisms of the different prevailing winds can most likely be obtained only through a detailed study of their diurnal and seasonal variations.

In the following section we try to understand if the bottom of mountain slopes around DPG are the most favourable areas, during the nighttime, for flow separation and convergence conducive to unusually vigorous mixing.

4 Nighttime processes: flow separation

In Section 3 we formulated the hypothesis that orographically induced modification of the ambient flow might foster low-level flow convergence and flow separation in the DPG area, in particular at night when the atmosphere is stably stratified near the ground.

Because the terms *convergence* and *separation* might seem unrelated to each other, or even contradictory, it is useful to clarify the definition of the latter. BLS occurs when a strong adverse pressure gradient force decelerates near-surface flow and eventually reverses its direction. As this happens, mass continuity requires the flow to be lifted off the surface, hence the concept of separation (Scorer 1958; Batchelor 1967). Near-surface wind vectors on opposite sides of the separation line converge into it, hence the approximate equivalence of the terms *convergence* and *separation* in the context of this section.

BLS is only one of many processes that might relate to flow convergence near the ground. Others include thermal updrafts developing over the crests of mountain ridges (Serafin and Zardi 2010), or even processes entirely unrelated to BL dynamics like fronts or gravity currents, i.e., bores or downdrafts generated by convective storms. However, BLS is the only process favouring convergence in a stable BL that would systematically occur in the immediate vicinity of topography features. This motivates the special emphasis given to this phenomenon in the present study.

Both (large-scale) dynamical forcing and (local-scale) thermal forcing can be responsible for flow separation at the bottom of a slope. Thermal forcing is primarily related to cold air pooling, leading to a positive pressure anomaly in the area where cold air accumulates. Integrating the hypsometric equation suggests that, for realistic cold pool depths and strengths, perturbations larger than 0.1 hPa should not be expected at DPG.

Dynamical forcing can cause different separation regimes (i.e., bluff-body separation at mountain top or wave-induced separation) which correspond to distinct ranges of values of two nondimensional parameters (Baines 1997; Ambaum and Marshall 2005). These are the mountain aspect ratio, h_m/L, (h_m being the mountain height and L its half-width) and the upstream nondimensional mountain height, Nh_m/U, (N being the Brunt-Väisälä frequency and U the ambient wind speed). Considering the aspect ratio of Granite Peak (~ 0.2), both separation regimes might occur in its lee, with a preference for wave-induced separation down the lee slope in the stable nocturnal environment. Negative pressure perturbations generated over the slope by mountain wave activity can easily exceed a few tenths of hPa (see below and Fig. 8-9 for examples), suggesting that dynamical forcing induces separation more likely than thermal forcing in this area.

A plausible scenario for the occurrence of BLS at DPG is the following. Under certain conditions, ambient flow over or around obstacles in a stable environment generates mountain waves. Pressure perturbations embedded in waves of sufficiently large amplitude force the BL to separate. Separation occurs downstream of a localized pressure minimum, i.e., in a region of adverse pressure gradient force, typically near the foot of lee slopes. Air upstream of the separation point, displaced downwards by the wave, is related to a warm anomaly because of adiabatic compression heating. Extremely stable air at the bottom of the lee side of mountains, if present, hydrostatically intensifies the adverse pressure gradient generated by the wave, further favouring the tendency to separation. Large gradients of wind speed, pressure, and temperature occur along the separation line. Evidence in support of this scenario is provided in what follows.

Detecting convergence lines related to flow separation from extensive sets of 4DWX model output requires analysing not only time series of near-surface wind fields, but also of pressure and temperature fields. An appropriate processing of pressure and temperature data proves to be necessary, in order to filter out their obvious altitudinal and seasonal variability. Our filtering method consists of two steps.

First, an areal average $\overline{\phi}^{xy}$ is removed from the original signal ϕ (a two-year time series of either pressure or temperature at one-hour intervals). The detrended signal ϕ'' is defined as $\phi''(x,y,t) = \phi(x,y,t) - \overline{\phi}^{xy}(t)$. This step essentially removes the fingerprint of synoptic systems, which cause time-dependent but approximately homogeneous temperature and pressure perturbations in the relatively small DPG area. The result is a set of detrended time series (one per each grid point in the 4DWX domain) or, in other words, a map of time series.

Second, the detrended signal ϕ'' is subjected to high-pass temporal Lanczos filtering, yielding the filtered signal ϕ'. The Lanczos method is a filtering approach in Fourier space which significantly reduces the Gibbs phenomenon, i.e., the appearence in the filtered series of spurious under- and overshoots near sharp discontinuities. Originally introduced in the field of meteorology (Duchon 1979), in more recent years Lanczos filtering has gained wide popularity in a number of disciplines including image processing. High-pass filtering removes from ϕ'' any oscillatory behaviour related to seasonal or diurnal variability (a cutoff frequency of 1/12 hr^{-1} was adopted in this study). The resulting filtered signal ϕ' only retains the fingerprint of high-frequency or intermittent atmospheric disturbances. Time series from all grid points are treated independently from each other during this stage.

The effects of this two-step filtering at seasonal and diurnal scales are illustrated in Fig. 7, which shows time series at two 4DWX grid points, one on top of Granite Peak, another a few km east of it. Removal of area-wide trends from the pressure field leaves discernible altitudinal, seasonal, and diurnal signals in p'' (Fig. 7a–c). The pressure perturbation is negative on the mountain top and positive on the lowland. Furthermore, the pressure difference between mountain top and lowland is smaller in summer and at daytime, which can be understood from the hypsometric equation (the larger the temperature, the smaller the pressure difference between two height levels). Lanczos filtering, resulting in the time series p', removes all of these sources of variability. Similar reasoning is valid for the temperature series in Fig. 7b–d.

{Figure 7 here}

Although time series from each grid point are treated independently during the Lanczos filtering step, filtered fields (i.e., maps) maintain spatial coherence, as shown in Figs. 8–9. The two examples show how filtering p and T data makes the distinctive features of flow separation apparent. In Fig. 8, the ambient flow is northerly and relatively strong northeasterly downslope flow occurs on the SW slope of the Cedar Mountains. A warm anomaly in the unfiltered T field, co-located with the region of high wind speeds, is apparent. However, no obvious relationship is visible between the wind field and the unfiltered p field, which only shows a distinct altitudinal fingerprint. After detrending and filtering, the temperature contrast along the downslope flow front is intensified, while a negative pressure perturbation ($p' < -0.5$ hPa) appears on the SW slope of the Cedar Mountains. The downslope flow reacts to the adverse pressure gradient force encountered at the foot of the slope by separating. Analogous dynamics are apparent in Fig. 9 which, however, refers to a case with southerly ambient flow. In these conditions, dynamically forced downslope flow occurs on the NE slopes of Granite Peak and the Dugway Range. Even in this case, downslope flow acceleration and separation are related to localized pressure minima on the lee sides of mountains, while a strong temperature contrast is present across the separation line.

{Figure 8 here}

{Figure 9 here}

The previous examples illustrate how dynamical forcing leads to the characteristic occurrence of strong and approximately co-located gradients of surface wind speed, pressure, and temperature in the vicinity of mountain slopes during BLS events. Gradient magnitude is easily computed from surface 4DWX output at each grid point and every output time, so a climatographical evaluation of where the strongest wind speed, temperature, and pressure contrasts occur in the DPG area is possible. Our sample consists of $\sim 3.21 \times 10^7$ elements (44 grid points along the x and y directions, and 16588 output times). For each point in the sample, the magnitudes of the horizontal gradients of the wind speed, temperature, and pressure are computed. The 99th percentiles of the three frequency distributions are then found. $||\nabla U||_{99}$, $||\nabla T||_{99}$, and $||\nabla p||_{99}$

correspond respectively to 2.57×10^{-3} s^{-1}, 6.34×10^{-4} K m^{-1}, and 7.59×10^{-5} hPa m^{-1}. These seemingly small numbers are actually orders of magnitude larger than typical synoptic-scale values. Also, $||\nabla p||_{99}$ is considerably larger than the horizontal pressure gradient that would result by integrating $||\nabla T||_{99}$ over a reasonable depth, further supporting the idea that flow separation on lee slopes is primarily dynamically driven.

The spatial distributions of simulated gradient magnitudes larger than $||\nabla U||_{99}$, $||\nabla T||_{99}$, and $||\nabla p||_{99}$ can be evaluated, and results of this elaboration are reported in Fig. 10. If extreme values were uniformly distributed over the DPG domain, the frequency of exceedence of the 99th percentile would be everywhere equal to 1%. Instead, there is a large degree of spatial variability.

{Figure 10 here}

The strongest wind speed, temperature, and pressure contrasts tend to occur at the foot of mountains (u and T fields) or on the low stretches of slopes (p field), consistent with flow separation slightly downstream of a pressure minimum (Fig. 10a,c,e). The bulk of BLS occurs during the night, as evinced by the fact that the nighttime fraction of strong wind speed and pressure gradients is largely above 50% near mountain flanks (Fig. 10b,d,f). The northeastern slopes of Granite Peak and the Dugway Range are hot spots, likely because of the dominance of southerly flows in the wind climatography of this area (see Section 3 above). In a nocturnal stable environment, frictional veering of southerly flows (see again Section 3) would favour the preferential onset of BLS on NE slopes; in this scenario, while low-level southerly winds are blocked, southwesterly winds at mountain-top level plunge down the mountain slopes.

Extreme value statistics from 4DWX data and Mini-SAMS observations, and their spatial distributions, are compared in Fig. 11. The period between 15 September and 29 October 2012 is considered (MATERHORN Fall 2012 field campaign), and percentiles are computed separately for the two datasets. Gradients from the Mini-SAMS network are computed from one-sided differences between each station and its NE and SE neighbors.

The distribution of extreme gradients in the 4DWX sample during the MATERHORN campaign is very similar to that of the complete 2012–2014 period (Fig. 10), with maximum frequencies concentrated along the NE slopes of the ridges.

Mini-SAMS stations are distributed over a predominantly flat area NE of the Dugway Range and E of Granite Peak, a few km away from their sidewalls. Therefore, they do not cover the regions were flow separation and convergence are more likely to happen, according to 4DWX simulations. However the general trend, with the frequency of intense wind speed gradients increasing E to W, and substantially doubling between the two sides of the network, is in good agreement with the model climatography, lending it further credence.

{Figure 11 here}

To summarize, S or SW flows with considerable near-surface frictional veering appear to be the most likely scenario leading to leeside BLS in DPG. Separation lines along the NE slopes of Granite Peak and the Dugway Range would constitute convergence zones, where dynamically accelerated flow on the steep mountain flanks interacts with drainage flow developing over the gently sloping plain. The resulting collision of air masses is expected to lead to considerable turbulence and enhanced mixing (Dimitrova et al 2015; El-Madany et al 2014).

5 Discussion and conclusions

In this paper, a set of simulations from a limited-area weather prediction model from 2012–2014 is analyzed in order to acquire insight into yet poorly understood aspects of nocturnal BL circulations in an area with complex topography and land cover, Dugway Proving Ground in northwestern Utah.

Mesoscale numerical weather prediction models are run operationally by many institutions around the world, primarily for the purpose of forecasting. In this context, long-term archives of past model simulations are normally employed for forecast verification. In contrast, examples of climatographical analysis of past operational mesoscale model output are uncommon. Some are related to the study of the spatial and interannual variability of rainfall (e.g., Hahmann et al 2009) or to the assessment of wind energy potential (Nawri et al 2014; Santos-Alamillos et al 2014).

Our study focuses instead on nocturnal atmospheric boundary-layer phenomena and aims to quantify the impact of mesoscale topography on airflow patterns. Regular thermally- or dynamically-driven circulations, which spring from characteristics of the land surface (like topography or thermal properties), have long offered the promise that mesoscale numerical weather prediction models can skillfully simulate this type of phenomena, at least in a climatological sense.

We demonstrate that 4DWX simulations offer an accurate representation of the prevalent wind directions and typical wind speeds observed at several locations across Dugway Proving Ground, as well as of their diurnal variability. Based on this outcome, we rely on 4DWX model output to describe some impacts of topography on the wind field in DPG.

The most frequent surface wind regimes at DPG correspond to southerlies and northwesterlies. In both cases, considerable veering (exceeding 45°) is typically observed in the lowest km of the atmospheric column, especially during the night. As expected, topography appears to modify these two basic patterns in various ways, e.g., by (a) diverting flow around obstacles, (b) promoting near-surface drainage of cold air, and (c) favouring wind acceleration on lee-side slopes in certain flow regimes. In the latter case, flows often converge at the bottom of slopes, in particular on the northeastern walls of mountains. These topographically induced convergence areas display the distinctive features of flow separation (i.e., strong gradients of wind speed, temperature, and pressure).

The plausibility of these results needs to be evaluated carefully, in view of the typical limitations of mesoscale weather models. Pointwise comparison of wind fields from 4DWX simulations and observational data supports the conclusion that the modelled and observed wind climates are indeed in very good agreement. However, it is worthwhile to mention that the simulations considered in the present study have a rather coarse resolution (1.1-km horizontal grid spacing) and rely on artificial numerical dissipation to remove noise and maintain stability in operational runs. Also, common BL parameterization schemes have a well-known tendency to be overdiffusive in nocturnal, very stable boundary layers (Grisogono 2010; Dimitrova et al 2015). All of these conspire to remove small-scale variability from solution fields and to damp spatial gradients. The absolute values of wind speed, temperature, and pressure gradients mentioned in this study should therefore not be interpreted absolutely. However, since the 1.1-km grid interval is more than sufficient to characterize many of the key features of orography, there is no reason to doubt that the spatial distribution of topographically induced gradients in the model fields are credibly reproduced in a climatological sense.

The value of the present results is essentially the spatially distributed information about BL flows at DPG with mesoscale detail. The planning of field activities there and at similar locations can benefit from this type of information. For instance, at DPG, it would be natural to concentrate on the foot of the E and NE slopes of Granite Peak and the Dugway Range to investigate the interaction between dynamically induced downslope winds and drainage flows.

As a concluding remark, we offer that the methods used for this study—the elaboration of climatographies of wind direction maps, extreme wind speed maps, and vertical atmospheric profiles; the high-pass filtering of pressure and temperature fields; and the study of spatial variability by considering gradient maps—are general enough to be easily applied in other contexts, provided that an equally extensive archive of mesoscale simulations is available.

Acknowledgements Matt Jeglum is thankfully acknowledged for sharing with the Authors his long-time experience as operational weather forecaster at DPG. His insightful comments helped improve this manuscript considerably. S. Serafin acknowledges support by the FWF (Austrian Science Fund) grant P24726-N27 to the University of Vienna (STABLEST, "Stable boundary layer separation and turbulence", PI S. Serafin). S.F.J. De Wekker acknowledges support from the Office of Naval Research Award # N00014-11-1-0709 J. Knievel acknowledges support from the U.S. Army Test and Evaluation Command, made possible through an interagency agreement with the National Science Foundation, which sponsors NCAR.

References

Ambaum MH, Marshall DP (2005) The effects of stratification on flow separation. J Atmos Sci 62:2618–2625

Baines PG (1997) Topographic effects in stratified flows. Cambridge University Press

Batchelor G (1967) An introduction to fluid dynamics. Cambridge University Press

Chen F, Dudhia J (2001) Coupling an advanced land surface-hydrology model with the Penn State-NCAR MM5 modeling system. Part I: Model implementation and sensitivity. Mon Wea Rev 129:569–585

Davis C, Warner T, Astling E, Bowers J (1999) Development and application of an operational, relocatable, mesogamma-scale weather analysis and forecasting system. Tellus A 51:710–727

De Wekker SFJ, Serafin S, Knievel JC (2015) A mesoscale model-based climatography of daytime boundary layer heights over the complex terrain of northwestern Utah. Bound-Layer Meteorol –:submitted

Dimitrova R, Silver Z, Zsedrovits T, Hocut C, Leo LS, Di Sabatino S, Fernando H (2015) Application of MATERHORN data to assess WRF boundary-layer schemes. Bound-Layer Meteorol –:submitted

Duchon CE (1979) Lanczos filtering in one and two dimensions. J Appl Meteor 18:1016–1022

Dudhia J (1989) Numerical study of convection observed during the Winter Monsoon Experiment using a mesoscale two-dimensional model. J Atmos Sci 46:3077–3107

El-Madany TS, Duarte HF, Durden DJ, Paas B, Deventer MJ, Juang JY, Leclerc MY, Klemm O (2014) Low-level jets and above-canopy drainage as causes of turbulent exchange in the nocturnal boundary layer. Biogeosciences 11:4507–4519

Epifanio C (2003) Lee vortices. In: Holton J, Pyle J, Curry J (eds) Encyclopedia of the Atmospheric Sciences, Cambridge University Press, pp 1150–1160

Fernando HJS, Pardyjak ER, Di Sabatino S, Chow FK, DeWekker SFJ, Hoch SW, Hacker J, Pace JC, Pratt T, Pu Z, Steenburgh JW, Whiteman CD, Wang Y, Zajic D, Balsley B, Dimitrova R, Emmitt GD, Higgins CW, Hunt JCR, Knievel JC, Lawrence D, Liu Y, Nadeau DF, Kit E, Blomquist BW, Conry P, Coppersmith RS, Creegan E, Felton M, Grachev A, Gunawardena N, Hang C, Hocut CM, Huynh G, Jeglum ME, Jensen D, Kulandaivelu V, Lehner M, Leo LS, Liberzon D, Massey JD, McEnerney K, Pal S, Price T, Sghiatti M, Silver Z, Thompson M, Zhang H, Zsedrovits T (2014) The MATERHORN – Unraveling the intricacies of mountain weather. Bull Amer Meteor Soc p submitted

French J, Haimov S, Oolman L, Grubišić V, Serafin S, Strauss L (2015) Wave-induced boundary-layer separation in the lee of the Medicine Bow Mountains. Part I: Observations. J Atmos Sci p submitted

Grisogono B (2010) Generalizing z-less mixing length for stable boundary layers. Quart J Roy Meteor Soc 136:213–221

Grisogono B, Belušić D (2009) A review of recent advances in understanding the meso and microscale properties of the severe Bora wind. Tellus 61A:1–16

Grubišić V, Doyle JD, Kuettner J, Dirks R, Cohn SA, Pan LL, Mobbs S, Smith RB, Whiteman CD, Czyzyk S, Vosper S, Weissmann M, Haimov S, De Wekker SFJ, Chow FK (2008) The Terrain-induced Rotor Experiment. Bull Amer Meteor Soc 89:1513–1533

Grubišić V, Serafin S, Strauss L (2015a) Climatology of westerly wind events in the lee of the Sierra Nevada. J Appl Meteorol Clim p submitted

Grubišić V, Serafin S, Strauss L, Haimov S, French J, Oolman L (2015b) Wave-induced boundary-layer separation in the lee of the Medicine Bow Mountains. Part II: Modeling. J Atmos Sci p submitted

Hahmann AN, Rostkier-Edelstein D, Warner TT, Vandenberghe F, Liu Y, Babarsky R, Swerdlin SP (2009) A reanalysis system for the generation of mesoscale climatographies. J Appl Meteor Climatol 49:954–972

Hong SY, Noh Y, Dudhia J (2006) A new vertical diffusion package with an explicit treatment of entrainment processes. Mon Wea Rev 134:2318–2341

Janjič ZI (2002) Nonsingular implementation of the Mellor-Yamada level 2.5 scheme in the NCEP meso model. Tech. rep., NCEP, National Centers for Environmental Prediction, Office Note No. 437

Kain JS (2004) The Kain-Fritsch convective parameterization: An update. J Appl Meteor 43:170–181

Knievel JC, Bryan GH, Hacker JP (2007) Explicit numerical diffusion in the WRF model. Mon Wea Rev 135:3808–3824

Lilly DK (1978) A severe downslope windstorm and aircraft turbulence event induced by a mountain wave. J Atmos Sci 35:59–77

Lin YL (2007) Mesoscale Dynamics. Cambridge University Press

Liu Y, Warner T, Bowers J, Carson L, Chen F, Clough C, Davis C, Egeland C, Halvorson S, Huck T, Lachapelle L, Malone R, Rife D, Sheu RS, Swerdlin S, Weingarten D (2008) The operational mesogamma-scale analysis and forecast system of the U.S. Army Test and Evaluation Command. Part I: Overview of the modeling system, the forecast products, and how the products are used. J Appl Meteor Climatol 47:1077–1092

Mayr GJ, Armi L, Gohm A, Zngl G, Durran DR, Flamant C, Gaberek S, Mobbs S, Ross A, Weissmann M (2007) Gap flows: Results from the mesoscale alpine programme. Quart J Roy Meteor Soc 133:881–896

Mlawer E, Taubman S, Brown P, Iacono M, Clough S (1997) Radiative transfer for inhomogeneous atmospheres: RRTM, a validated correlated-k model for the longwave. J Geophys Res 102(D14):16,663–16,682

Nappo C (2013) An Introduction to Atmospheric Gravity Waves. International geophysics series, Academic Press/Elsevier

Nawri N, Petersen GN, Bjornsson H, Hahmann AN, Jónasson K, Hasager CB, Clausen NE (2014) The wind energy potential of Iceland. Renewable Energy 69:290–299

Physick WL, Tapper NJ (1990) A numerical study of circulations induced by a dry salt lake. Mon Wea Rev 118:1029–1042

Rife DL, Warner TT, Chen F, Astling EG (2002) Mechanisms for diurnal boundary layer circulations in the Great Basin desert. Mon Wea Rev 130:921–938

Santos-Alamillos FJ, Pozo-Vázquez D, Ruiz-Arias JA, Lara-Fanego V, Tovar-Pescador J (2014) A methodology for evaluating the spatial variability of wind energy resources: Application to assess the potential contribution of wind energy to baseload power. Renewable Energy 69:147–156

Scorer R (1958) Natural aerodynamics. Pergamon Press

Serafin S, Zardi D (2010) Daytime heat transfer processes related to slope flows and turbulent convection in an idealized mountain valley. J Atmos Sci 67:3739–3756

Sharman RD, Liu Y, Sheu RS, Warner TT, Rife DL, Bowers JF, Clough CA, Ellison EE (2008) The operational mesogamma-scale analysis and forecast system of the U.S. Army

Test and Evaluation Command. Part III: Forecasting with secondary-applications models. J Appl Meteor Climatol 47:1105–1122

Skamarock W, Klemp J (2008) A time-split nonhydrostatic atmospheric model for weather research and forecasting applications. J Comput Phys 227:3465–3485

Thompson G, Rasmussen RM, Manning K (2004) Explicit forecasts of winter precipitation using an improved bulk microphysics scheme. Part I: Description and sensitivity analysis. Mon Wea Rev 132:519–542

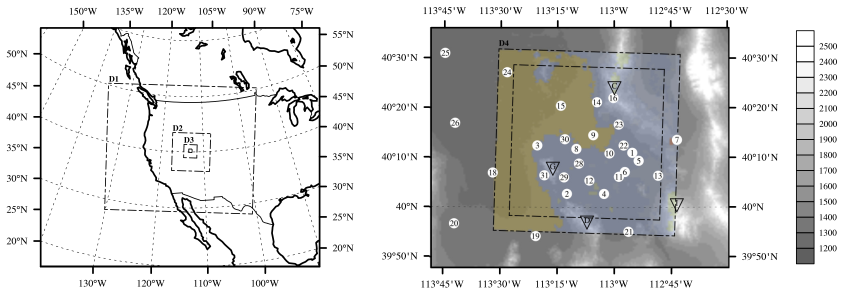

Fig. 1 Map of the study area. The diagram on the left shows the four domains of the 4DWX Dugway Proving Ground (DPG) simulations. On the right is a zoom-in on the DPG area, with grey shading representing surface altitude in m MSL and colors referring to land-cover categories. Two squares (dot-dashed lines) are drawn in the map. The larger one outlines the boundaries of 4DWX domain 4; the smaller one outlines the part of the domain that is not subject to flow relaxation towards the lateral boundaries. Numbers in white circles denote the position of SAMS automatic weather stations (stations 17 and 27, missing in the map, are located farther to the north). Letters in the down-pointing triangles refer to the major orography features in the area: Granite Peak (G, 2148 m MSL), the Cedar Mountains (C, 2110 m MSL), the Dugway Range (D, 2082 m MSL), and Indian Peaks (I, 2566 m MSL).

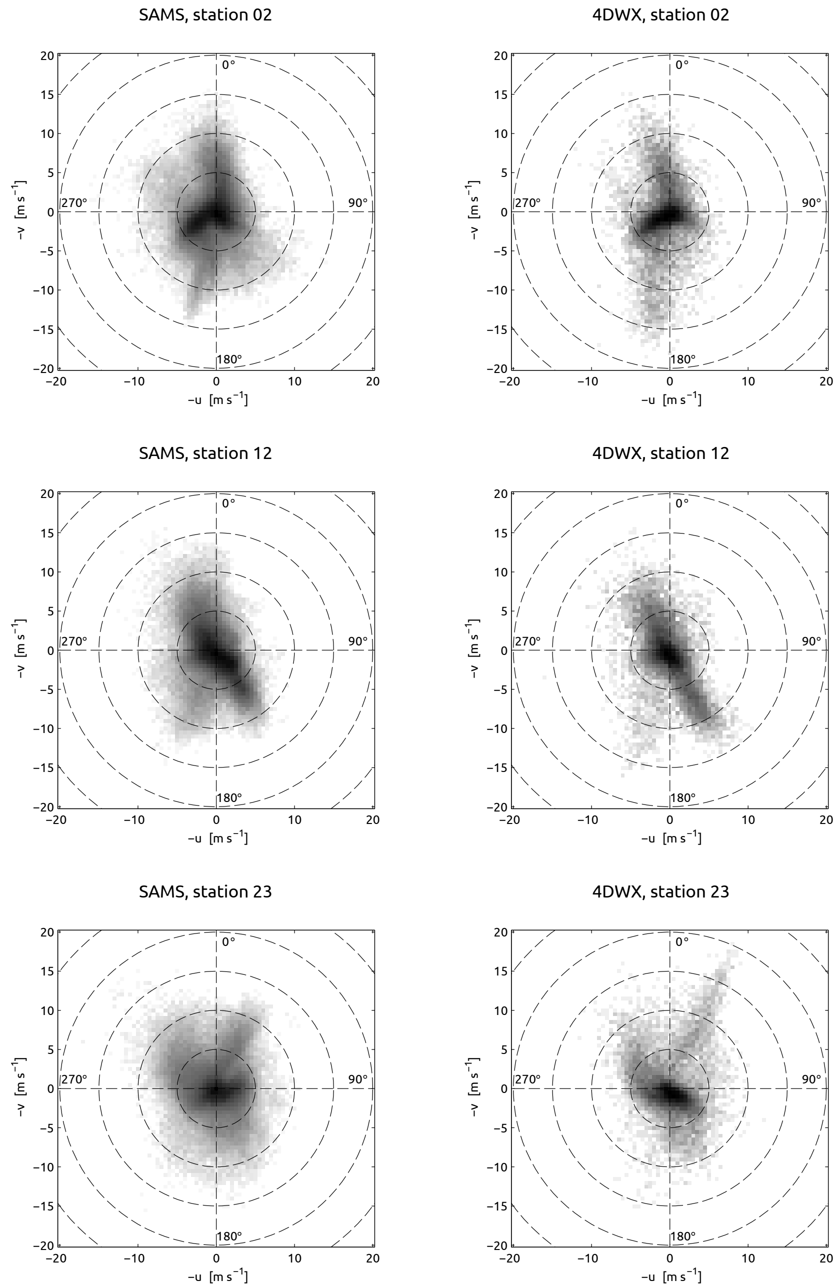

Fig. 2 Two-dimensional histograms of 10-m wind components u versus v at SAMS stations 2, 12, and 23, and at the corresponding nearest-neighbor 4DWX grid points. Relative frequencies in each histogram sum up to 100%. The color scale is proportional to the population of bins and is logarithmic in order to make even rare events clearly visible. Highly populated bins are displayed in darker shading.

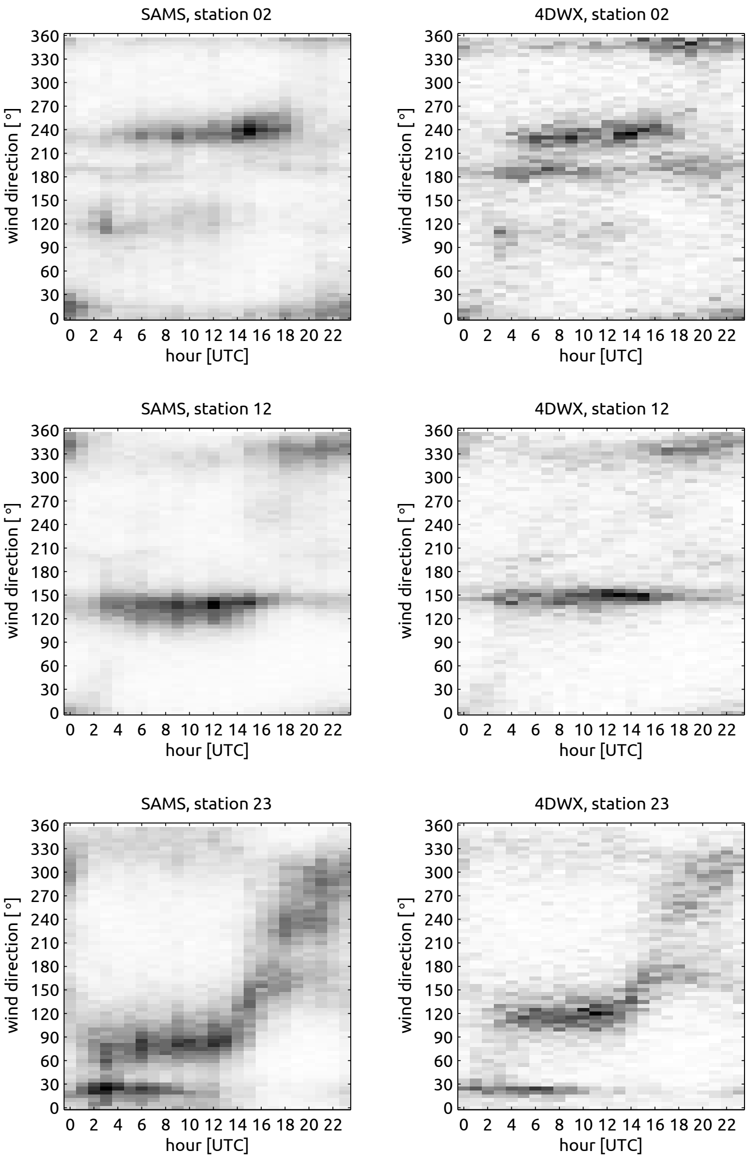

Fig. 3 As in Fig 2, but for the frequency of occurrence of 10-m wind speed > 1 m s^{-1} as a function of wind direction and time of day.

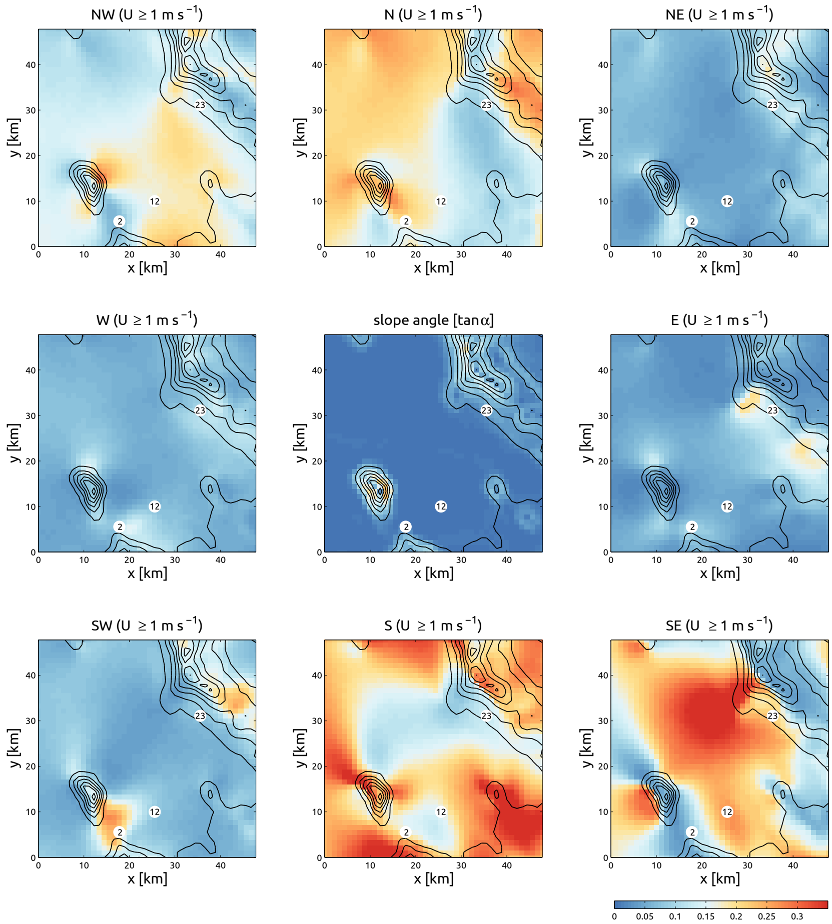

Fig. 4 Relative frequency of near-surface wind direction in eight directional sectors in 4DWX domain 4. Sectors are 45° wide and are centered on directions ranging from 0° (N) to 315° (NW). At each model gridpoint, frequencies from the eight directional sectors sum up to 100%. Only wind speeds > 1 m s^{-1} are considered. The slope angle ($\tan\alpha$) is represented in the middle panel. Isolines in all panels refer to surface altitude. The spacing between contours is 100 m. The color bar at the bottom left refers to frequencies in the range [0, 1] and applies to all panels.

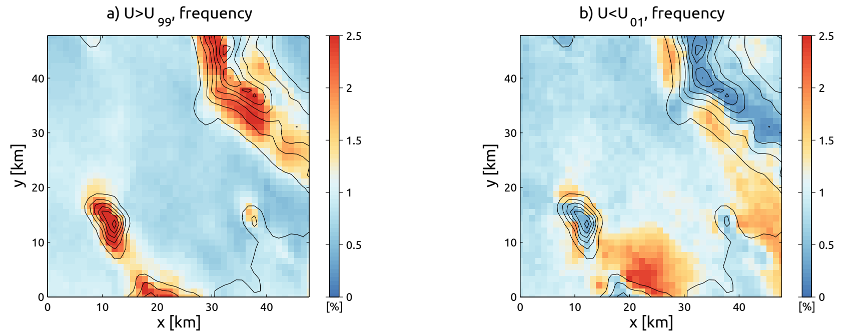

Fig. 5 Two-dimensional histograms representing the spatial distribution of extreme wind speed values (highs in *a* and lows in *b*). The frequency of exceedance (resp. not exceedance) of the 99th (resp. 1st) percentile is represented. A spatially uniform distribution of extremes would correspond to a uniform value of 1.

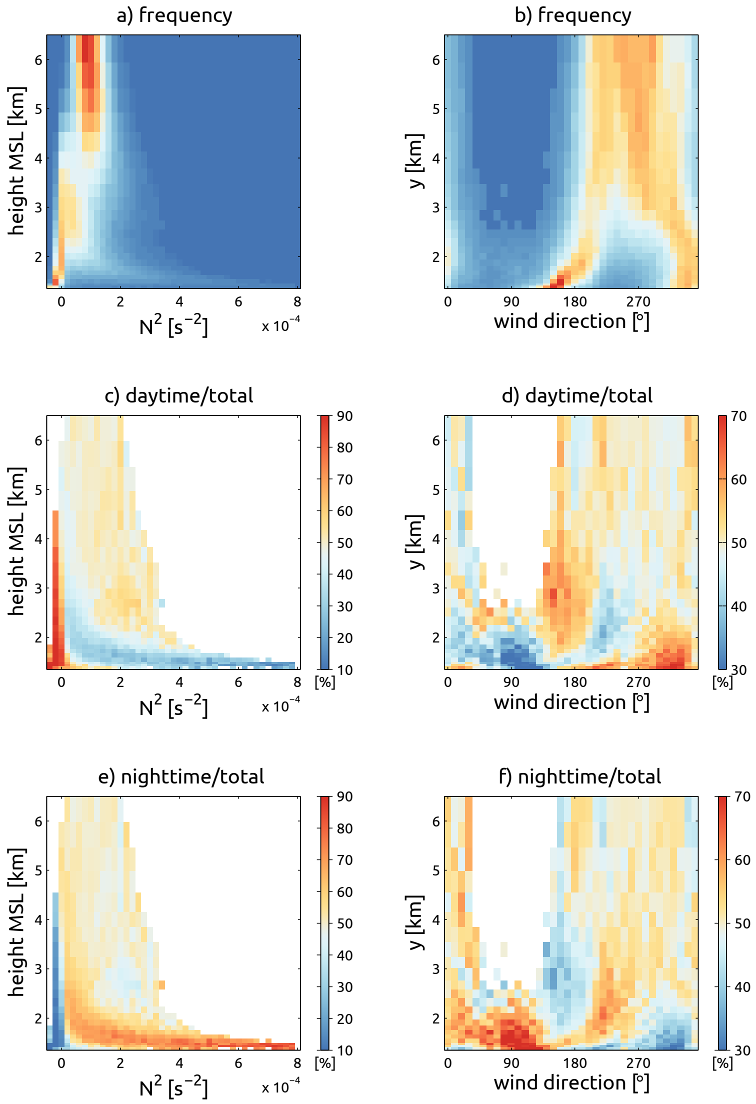

Fig. 6 Two-dimensional histograms representing the variability of the (*a*) Brunt-Vïsälä frequency and (*b*) wind direction with height MSL. Relative frequencies in each of histograms *a* and *b* sum up to 100%. Panels *c* and *d* represent the fraction of daytime events with respect to the total in each bin of panels *a* and *b*. Panels *e* and *f* represent instead the fraction of nighttime events. Corresponding bins in panels *c* and *e* sum up to 100%. The same applies to panels *d* and *f*. White areas in panels *c*–*f* correspond to scarcely populated bins.

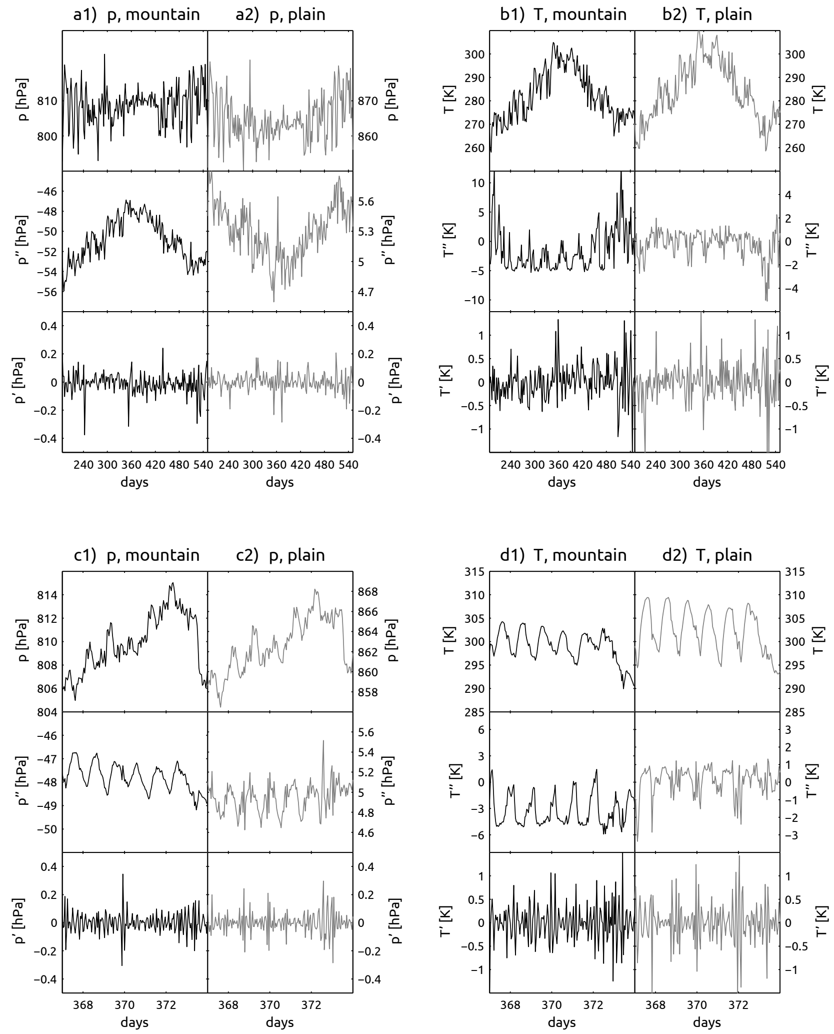

Fig. 7 Effect of filtering on pressure and temperature time series from 4DWX model output. Pressure, p, is the original series, p'' the result of detrending, and p' the result of Lanczos low-pass filtering. Panels a and b show the effects of filtering at annual scale. Panels c and d refer instead to the diurnal scale.

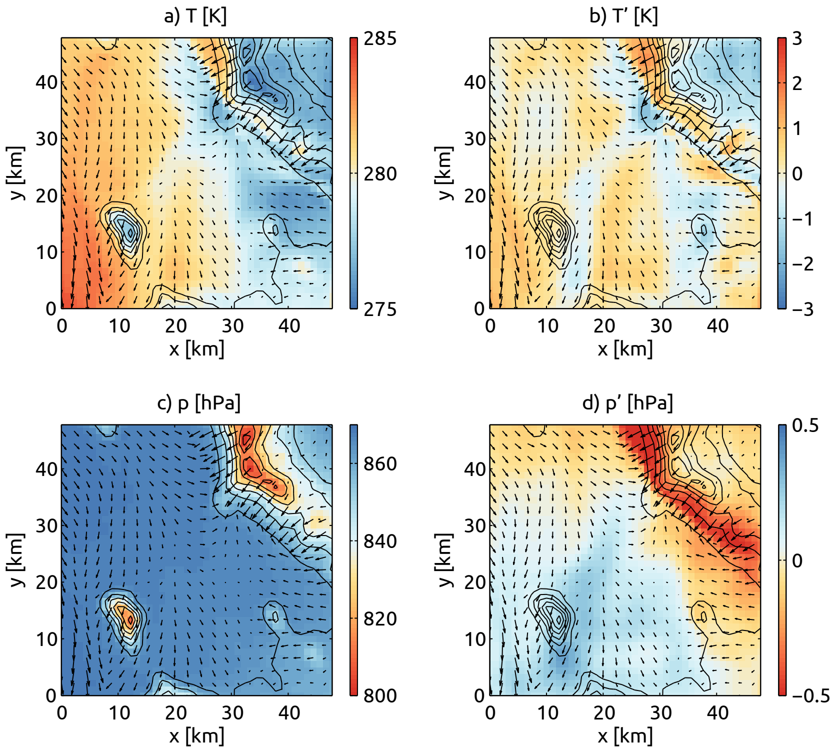

Fig. 8 Example of (*a* and *c*) unfiltered and (*b* and *d*) filtered temperature and pressure fields in the core of 4DWX domain 4. Vectors represent the wind field at the first model level above ground. Plots refer to model output on 12 May 2014 at 0900 UTC (0200 LST).

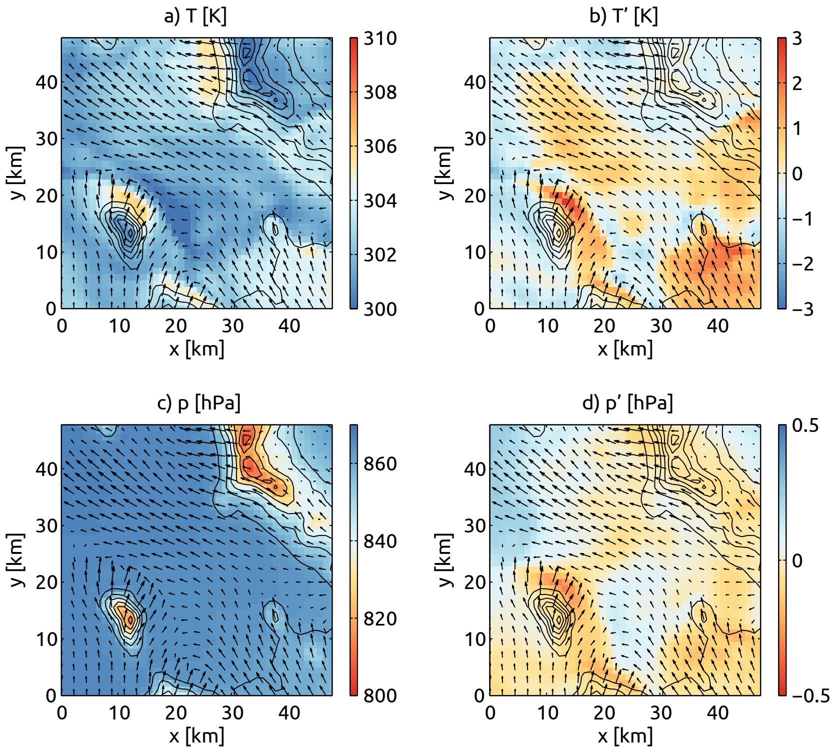

Fig. 9 As in Fig. 8, but for 8 August 2012 at 0700 UTC (0000 LST).

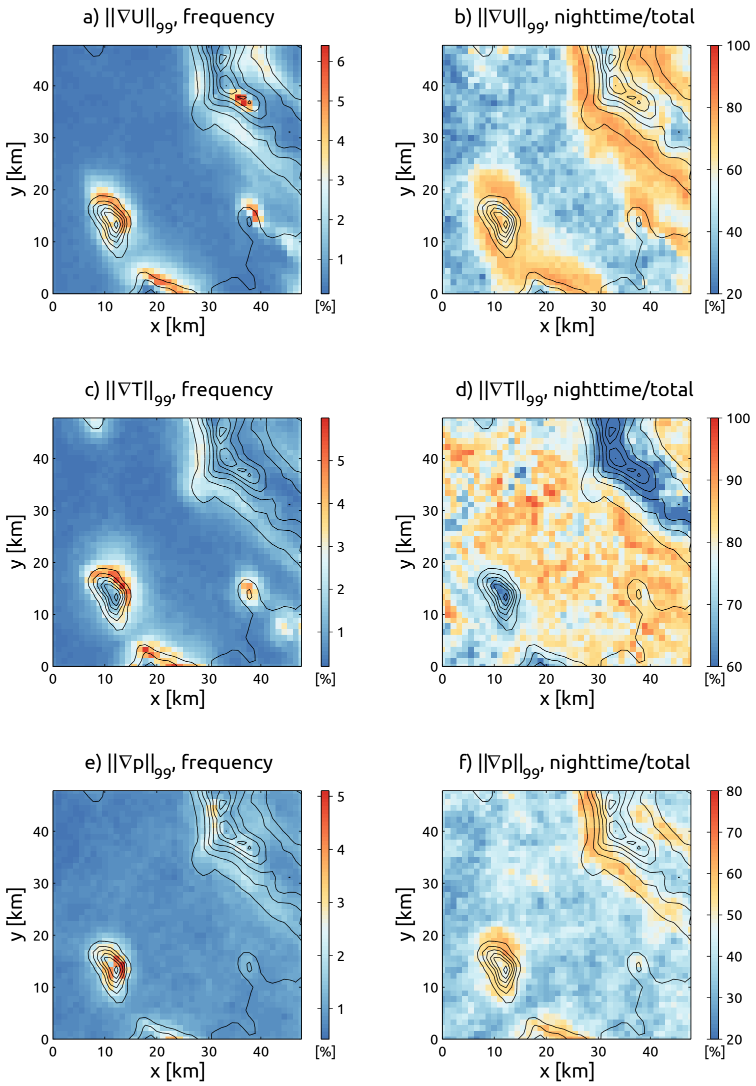

Fig. 10 Two-dimensional histograms representing the spatial distribution of extreme values of the magnitude of the gradients of (*a*) wind speed, (*c*) filtered temperature, and (*e*) filtered pressure. Relative frequencies in each of histograms *a*, *c*, and *e* sum up to 100%. Panels *b*, *d*, and *f* represent the fraction of nighttime events with the respect to the total in each bin of panels *a*, *c*, and *e*, respectively.

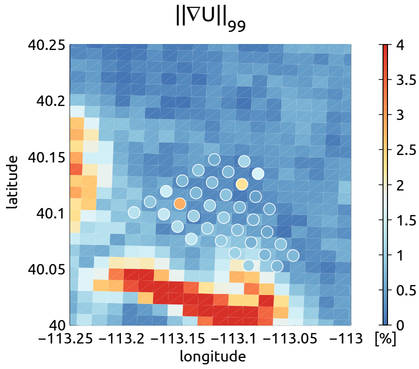

Fig. 11 Comparison between observed (Mini-SAMS, colored bullets) and modelled (4DWX, background gridded map) wind speed gradient climatographies at DPG during a period of the MATERHORN fall 2012 field campaign (15 September to 29 October). Colors represent the spatial distribution of extreme values of the magnitude of the wind speed gradients (i.e., of the samples for which wind speed gradient exceeds the 99th percentile of its frequency distribution, in each of the two datasets). The temporal interval of the samples is 1 hour for 4DWX and 1 minute for Mini-SAMS.